Structural and Biochemical Characterization of the GTPγS-, GDP·P_i-, and GDP-Bound Forms of a GTPase-Deficient $Gly^{42} \rightarrow Val$ Mutant of $G_{i\alpha1}$[†]

Andre S. Raw,[‡] David E. Coleman,[§] Alfred G. Gilman,[‡] and Stephen R. Sprang*,[‖]

Departments of Pharmacology and Biochemistry and Howard Hughes Medical Institute, Department of Biochemistry, University of Texas Southwestern Medical Center, Dallas, Texas 75235

Received August 4, 1997; Revised Manuscript Received October 6, 1997[⊗]

ABSTRACT: The $Gly^{42} \rightarrow Val$ mutant of $G_{i\alpha1}$ was characterized structurally and biochemically to elucidate two important features of $G_{i\alpha1}$-catalyzed GTP hydrolysis. The crystal structure of the GTPγS-bound $G^{42}VG_{i\alpha1}$ protein demonstrates that the steric bulk of Val^{42} pushes the Gln^{204} residue into a catalytically incompetent conformation, providing a rationale for the diminished GTPase activity of this mutant. The same phenomenon may also account for the diminished GTPase activity of the homologous transforming $Gly^{42} \rightarrow Val$ mutation in $p21^{ras}$. Similarly, the steric bulk of the unique Ser^{42} residue in $G_{z\alpha}$ may account for the comparatively slower rate of GTP hydrolysis by this G_α subunit. The $G^{42}VG_{i\alpha1}$ subunit was also characterized structurally in its GDP·P_i- and GDP-bound states, providing a unique opportunity to view three "snapshots" of GTP hydrolysis. Hydrolysis of GTP to a transient GDP·P_i-bound intermediate is associated with substantial conformational changes in the switch II segment of the protein. Eventual release of P_i results in further removal of switch I from the active site and a highly mobile switch II segment. Despite their disparate biochemical properties, the structural similarity of $G^{42}VG_{i\alpha1}$ to the $G^{203}AG_{i\alpha1}$ mutant in the GDP·P_i-bound form suggests that both mutations stabilize a conformation of the GDP·P_i-bound protein that occurs only transiently in the wild-type protein. The structures of the GDP-bound forms of the wild-type and mutant proteins are similar.

Transient, high-affinity interactions between GTP and the α subunits of heterotrimeric guanine nucleotide-binding regulatory proteins (G proteins)[1] activate the downstream signaling reactions that are initiated by these molecules (*1*−*5*). Binding of GTP to G_α is catalyzed by an appropriate agonist−receptor complex, which facilitates dissociation of tightly bound GDP from the G protein heterotrimer. GTP, present in cells at much higher concentrations than GDP, fills the empty nucleotide binding site and causes conformational changes that result in dissociation of G_α(GTP) from a high-affinity dimer of β and γ subunits (*6*). The intrinsic GTPase activity of G_α eventually regenerates G_α(GDP), and subsequent binding of $G_{\beta\gamma}$ completes the cycle.

The GTPase reaction catalyzed by a variety of regulatory GTPases has been studied extensively because of its intrinsic biological importance, revealed in part by the consequences of its inhibition. Thus, cholera toxin-catalyzed ADP-ribosylation of the G_α protein responsible for stimulation of adenylyl cyclase ($G_{s\alpha}$) inhibits its GTPase activity (*7*). Resultant persistent activation of the pathway causes uncontrolled synthesis of cyclic AMP and life-threatening diarrheal disease. Mutations in $p21^{ras}$ that inactivate the GTPase activity of this protein (and render it unsusceptible to the activity of GTPase-activating proteins or GAPs) cause a large number of human malignancies; the $Gly^{12} \rightarrow Val$ mutation of $p21^{ras}$ is the most common of these alterations (*8*, *9*).

Table 1: Conserved Phosphate-Binding Loop Motif[a]

human Ras	(10)	G A G G V G K S
bovine $G_{s\alpha}$	(47)	G A G E S G K S
bovine $G_{i\alpha}$	(40)	G A G E S G K S
bovine $G_{t\alpha}$	(36)	G A G E S G K S
bovine $G_{o\alpha}$	(40)	G A G E S G K S
human $G_{z\alpha}$	(40)	G T S N S G K S
mouse $G_{q\alpha}$	(40)	G T G E S G K S

[a] The number preceding the sequence corresponds to the first residue number of the motif.

Gly^{12} in $p21^{ras}$ is located in the so-called P loop (GXXXXGK sequence motif), which is involved in binding the α- and β-phosphates of nucleotides in many proteins (Table 1). Despite crystallographic studies that have documented the proximity of Gly^{12} to the catalytic Gln^{61} residue in $p21^{ras}$, the explanation for the catalytic inactivity of Val^{12}-$p21^{ras}$ remains unclear because the so-called switch II segment that includes Gln^{61} is poorly ordered (*10*−*12*). Most G_α proteins also have P-loops with a conserved Gly residue that is homologous to Gly^{12} of $p21^{ras}$. However, we originally felt that study of heterotrimeric G protein α subunits had little to contribute to the question of the importance of this Gly residue because the GTPase activity of the equivalent $Gly^{49} \rightarrow Val$ mutant of $G_{s\alpha}$ was only modestly diminished (*13*). We have reexamined this issue

[†] This work was supported by NIH Grant DK46371 and Welch Foundation Grant I-1229 (to S.R.S.) and NIH Grant GM34497 and Welch Foundation Grant I-1271 (to A.G.G.). A.G.G. also acknowledges support from the Raymond and Ellen Willie Distinguished Chair in Molecular Neuropharmacology.

* To whom correspondence should be addressed.

[‡] Department of Pharmacology.

[§] Department of Biochemistry.

[‖] Howard Hughes Medical Institute, Department of Biochemistry.

[⊗] Abstract published in *Advance ACS Abstracts,* December 1, 1997.

[1] Abbreviations: G proteins, heterotrimeric guanine nucleotide-binding proteins; GAP, GTPase-activating protein; GTPγS, guanosine 5′-(3-*O*-thiotriphosphate); $C_{12}E_{10}$, poly(oxyethylene) 10-lauryl ether. Mutant proteins are designated by the wild-type amino acid residue, the position of this residue, and the residue used for replacement.

S0006-2960(97)01912-0 CCC: $14.00

for several reasons. (1) The switch II segment in at least certain GTPγS-bound G_α proteins is well ordered compared to that of $p21^{ras}$ (*14*, *15*). (2) $G_{z\alpha}$, a member of the G_i subfamily of G_α subunits, is distinct because of very low GTPase activity (100-fold lower than $G_{s\alpha}$ or $G_{i\alpha}$) and a unique TSN sequence in the P-loop rather than the consensus AGE in other G_α proteins (*16*). (3) The $Gly^{203} \rightarrow$ Ala mutant of $G_{i\alpha1}$ (an unrelated Gly residue), a conformationally constrained protein, can be crystallized in an intermediate G_α(GDP·P_i) state but not in its active GTPγS-bound form (*17*). Wild-type $G_{i\alpha1}$ cannot be crystallized in its GDP·P_i-bound form. (4) $Gly^{42} \rightarrow$ Val $G_{i\alpha1}$ (analogous to $Gly^{12} \rightarrow$ Val $p21^{ras}$), which has severely impaired GTPase activity (see below), can be crystallized in all three GTPγS-, GDP-, and GDP·P_i-bound forms. Hence, this protein offers a unique opportunity to obtain three "snapshots" of guanine nucleotide binding and hydrolytic reactions as well as insights into the consequences of mutation at Gly^{42}.

MATERIALS AND METHODS

Proteins and Plasmids. A cDNA containing the entire coding sequence of rat $G_{i\alpha1}$ was ligated into the *Eco*RI site of M13mp19. Mutagenesis was performed by the method of Kunkel *et al.* (*18*). The complete coding sequences of the $G^{42}V$ and $G^{203}A$ mutants were confirmed by dideoxynucleotide sequencing. The complete coding sequences (*Nco*I−*Hin*dIII fragments) of the two mutants and the wild-type protein were subcloned into the *Nco*I and *Hin*dIII sites of plasmid pQE-6. Other P-loop mutants were subcloned into the *Nco*I and *Hin*dIII sites of plasmid H_6pQE-6 to generate proteins with hexahistidine sequences at their amino termini. These plasmids were transformed together with plasmid pREP4 into *Escherichia coli* BL21 (DE3) cells. Proteins were expressed and purified as previously described (*19*).

GTPγS Binding Kinetics. $G_{i\alpha1}$ proteins (200 nM) were incubated at 30 °C in 50 mM NaHepes (pH 8.0), 1 mM EDTA, 5 mM DTT, 0.05% $C_{12}E_{10}$, 10 mM $MgSO_4$, and 1 μM [^{35}S]GTPγS (3000 cpm/pmol). Aliquots (100 μL) were withdrawn at the indicated times, added to wash buffer at 0 °C (20 mM Tris-HCl, pH 8.0, 100 mM NaCl, and 25 mM $MgCl_2$), and applied to nitrocellulose filters (Schleicher and Schuell BA-85, 0.45 μm); filters were washed and bound radioactivity was quantified (*20*). Values of k_{app} were calculated by a nonlinear least-squares fit to $B = B_{eq}(1 - e^{-kt})$. Note that k_{app} is also eqiuvalent to the dissociation rate of GDP.

GTPγS Dissociation Kinetics. $G_{i\alpha1}$ proteins (200 nM) were incubated for 90 min with 1 μM [^{35}S]GTPγS as described above. GTP was then added to a final concentration of 200 μM. Aliquots (80 μL) were withdrawn at the indicated times and counted as previously described to quantify GTPγS binding. Values of k_{app} were calculated by a nonlinear least-squares fit to $B = B_o e^{-kt}$.

Steady-State Hydrolysis of GTP. $G_{i\alpha1}$ proteins (200 nM) were incubated at 30 °C in 50 mM NaHepes (pH 8.0), 1 mM EDTA, 5 mM DTT, 0.05% $C_{12}E_{10}$, 10 mM $MgSO_4$, and 2 μM [γ-^{32}P]GTP (3000 cpm/pmol). At the indicated times, aliquots (50 μL) were withdrawn, added to 750 μL of 5% (w/v) Norit in 50 mM NaH_2PO_4 (0 °C), and vortexed. The charcoal was removed by centrifugation (2000 rpm for 10 min in a Beckman JA 4.2 rotor). The radioactivity in a 400 μL aliquot of supernatant was quantified (*21*). Steady-state hydrolysis experiments were also performed with 50 mM NaMES (pH 5.6), 50 mM sodium phosphate (pH 8.0), or 50 mM sodium phosphate (pH 5.6) in place of 50 mM NaHepes (pH 8.0).

Measurement of k_{cat} for Hydrolysis of GTP. $G_{i\alpha1}$ proteins (400 nM) were incubated at 30 °C in 50 mM NaHepes (pH 8.0), 10 mM EDTA, 5 mM DTT, 0.05% $C_{12}E_{10}$, and 1 μM [γ-^{32}P]GTP (7000 cpm/pmol) for 30 min. Single turnover GTP hydrolysis reactions were then initiated by the addition of GTP and $MgSO_4$ to final concentrations of 100 μM and 20 mM, respectively. Aliquots (50 μL) were withdrawn at the indicated times and processed as described for the steady-state GTPase assay. Values of k_{cat} were calculated by a nonlinear least-squares fit to $B = B_{eq}(1 - e^{-kt})$. GAP-stimulated GTPase reactions were analyzed in an analogous fashion in the presence of 400 nM RGS4 (*22*).

Measurement of k_{pi} for Hydrolysis of GTP. $G_{i\alpha1}$ proteins (400 nM) were incubated at 30 °C in 50 mM NaHepes (pH 8.0), 10 mM EDTA, 5 mM DTT, 0.05% $C_{12}E_{10}$, and 1 μM [γ-^{32}P]GTP (10 000 cpm/pmol) for 30 min. Single turnover GTP hydrolysis reactions were then initiated by the addition of GTP and $MgSO_4$ to final concentrations of 100 μM and 20 mM, respectively. Aliquots (100 μL) were withdrawn at the indicated times, added to wash buffer at 0 °C (20 mM Tris-HCl, pH 8.0, 100 mM NaCl, and 25 mM $MgCl_2$), and filtered within 10 s using nitrocellulose filters as described above. Values of k_{pi} were calculated by a nonlinear least-squares fit to $B = B_o e^{-kt}$.

Measurement of Mg^{2+} Affinity. $G_{i\alpha1}$ proteins (300 nM) were incubated at 30 °C in 50 mM NaHepes (pH 8.0), 5 mM EDTA, 5 mM DTT, 0.05% $C_{12}E_{10}$, and 10 μM GTPγS for 3 h. This mixture was divided into 600 μL aliquots, and $MgSO_4$ was added (in 6 μL) to achieve the concentrations indicated. After 15 min at room temperature, intrinsic tryptophan fluorescence was measured with a SPEX Fluorolog 211 spectrophotometer using excitation and emission wavelengths of 289 and 349 nm, respectively (*23*). These data were fit to the equation $F = ax/(K_d + x)$, where F is Mg^{2+}-induced fluorescence enhancement, x is the concentration of Mg^{2+}, a is the maximum value $F(x)$, and K_d is the dissociation constant for Mg^{2+}.

Trypsinization. $G_{i\alpha1}$ proteins (8 μg/45 μL) in 50 mM NaHepes (pH 8.0), 1 mM EDTA, 5 mM DTT, 0.05% $C_{12}E_{10}$, and 10 mM $MgSO_4$ were incubated with either 100 μM GDP; 100 μM GDP, 10 mM NaF, and 60 μM $AlCl_3$; or 100 μM GTPγS for 3 h at 30 °C. *N*-Tosyl-L-phenylalanine chloromethyl ketone-treated trypsin (9 μL at 0.5 mg/mL) was then added, and this mixture was incubated for 15 min at room temperature. Trypsinization was stopped by addition of SDS−PAGE sample buffer and boiling. Samples were resolved on 11% SDS−polyacrylamide gels and stained with Coomassie Blue (*24*).

Crystallization. The GTPγS·Mg^{2+} complex of $G^{42}VG_{i\alpha1}$ was prepared by incubating the protein with 50 mM NaHepes (pH 8.0), 1.0 mM EDTA, 5 mM DTT, 0.05% $C_{12}E_{10}$, 10 mM $MgSO_4$, and 1.0 mM GTPγS for 4 h at 30 °C. The protein was further purified over a Mono-Q 10/10 column as described (*19*) and exchanged into 50 mM NaHepes (pH 8.0), 1.0 mM EDTA, 5 mM DTT, 10 mM $MgSO_4$, and 200 μM GTPγS (protein concentration 15−20 mg/mL). Hanging drops (7 μL) containing a 1:1 ratio of protein and buffer [$(NH_4)_2SO_3$ (1.5−2.0 M) and 100 mM sodium acetate (pH

Table 2: Data Collection Statistics for $G^{42}VG_{i\alpha1}$

parameter	GTPγS complex	GDP·P_i complex	GDP complex
resolution range (Å)	15−2.0	15−2.8	15−2.4
space group	$P3_221$	$P4_32_12$	$I4$
cell constants (Å)	$a = b = 78.95$, $c = 105.29$	$a = b = 77.19$, $c = 143.61$	$a = b = 121.44$, $c = 68.29$
unique reflections	19678	10403	19384
redundancy	2.3	2.8	3.6
completeness (%)	74.9[a]	93.1	99.3
R_{merge}[b] (%)	9.9	5.9	6.3
$\langle I\rangle/\langle\sigma\rangle$	10.4	15.4	20.5
temperature (K)	110	278	110
X-ray source	CHESS A1	rotating anode	CHESS F1

[a] Data to 2.5 Å resolution is 90% complete. [b] $R_{merge} = \sum_h\sum_i|I(h) - I(h)_i|/\sum_h\sum_i I(h)_i$.

Table 3: Refinement Statistics for $G^{42}VG_{i\alpha1}$

parameter	GTPγS complex	GDP·P_i complex	GDP complex
resolution range (Å)	8.0−2.0	8.0−2.8	8.0−2.4
R_{factor}[a] (%)	20.6	18.9	21.2
R_{free} (%)	25.9	25.0	27.4
atoms (N)	2650	2577	2780
waters (N)	90	5	64
deviation from ideality (rms)			
bonds (Å)	0.010	0.012	0.011
angles (deg)	1.536	1.650	1.534
Ramachandran plot[b]			
most favored (%)	94.4	90	93.7
favored (%)	5.6	10	6.3
generous or disallowed (%)	0	0	0

[a] R factor $= \sum|F_o - F_c|/\sum|F_o|$. R_{free} corresponds to the R factor for 10% of the reflections in the data set randomly excluded from refinement. Only reflections with $F/\sigma > 1.0$ were used in refinement. [b] Analysis from PROCHECK.

6.0)] were allowed to equilibrate against a reservoir (1.0 mL) of the same buffer. After 7 days at 20 °C, trigonal rods (0.10 mm × 0.10 mm × 0.60 mm) were obtained. These were serially transferred into stabilization solutions [70% saturated $LiSO_4$, 100 mM BES (pH 7.0), 5 mM DTT, 1 mM EDTA, 10 mM $MgSO_4$, 50 μM GTPγS] containing glycerol in 5% increments to a maximum of 20%. The crystals were mounted in a rayon loop and frozen in liquid nitrogen for data collection (*14*, *25*).

Crystals of the GDP·P_i-bound form of $G^{42}VG_{i\alpha1}$ were obtained by exchanging the protein into 50 mM NaHepes (pH 8.0), 1.0 mM EDTA, 5 mM DTT, 10 mM $MgSO_4$, and 5 mM GDP (protein concentration 10−15 mg/mL). Hanging drops (7 μL) containing a 1:1 ratio of protein and buffer (ammonium phosphate, 2.2−2.5 M, pH 5.5−5.8) were allowed to equilibrate against a reservoir (1.0 mL) of the same buffer. After 7 days at 20 °C, tetragonal rods (0.20 mm × 0.20 mm × 0.80 mm) were obtained. Crystals were mounted directly from the mother liquor for data collection (*17*).

Crystals of the GDP-bound form of $G^{42}VG_{i\alpha1}$ were obtained by exchanging the protein into 50 mM NaHepes (pH 8.0), 1.0 mM EDTA, 5 mM DTT, and 5 mM GDP (protein concentration 10−15 mg/mL). Tetragonal rods (0.10 mm × 0.10 mm × 0.60 mm) were obtained and frozen as described for the GTPγS-bound protein.

X-ray Data Collection, Model Building, and Refinement. Data sets (Table 2) for the GTPγS·Mg^{2+} and GDP forms of $G^{42}VG_{i\alpha1}$ (110 K) were obtained at the Cornell High Energy Synchrotron Source (CHESS) beamline equipped with a 2K CCD detector. Data for the GDP·P_i form of $G^{42}VG_{i\alpha1}$ (5 °C) were obtained with a Raxis II imaging plate system equipped with a RU300 X-ray generator. The data were integrated and indexed with DENZO and scaled with SCALEPACK (*26*). Crystals of $G^{42}VG_{i\alpha1}$(GTPγS·Mg^{2+}) and $G^{42}VG_{i\alpha1}$(GDP) were isomorphous to corresponding crystals of the wild-type protein. Likewise, crystals of $G^{42}VG_{i\alpha1}$(GDP·P_i) were isomorphous to crystals of $G^{203}AG_{i\alpha1}$(GDP·P_i). Hence, the GTPγS·Mg^{2+} and GDP forms of $G_{i\alpha1}$ and the GDP·P_i form of $G^{203}AG_{i\alpha1}$ were used as initial phasing models. The calculated phases were combined with the amplitudes for the measured reflections from $G^{42}VG_{i\alpha1}$. After rigid body and simulated annealing refinement (X-PLOR) (*27*), SigmaA-weighted (*28*) simulated annealing omit maps were used to refit regions around the active site. Using the free R factor to monitor the reliability of the convergence, cycles of minor rebuilding (modeling program O) (*29*), further refinement, and placement of solvent molecules resulted in the final models. Each of the three models displays good stereochemistry with at least 90% of the residues in the most favored regions of the Ramachandran plot and with none in the generous or disallowed regions (PROCHECK) (*30*). Data collection and refinement statistics are shown in Tables 2 and 3. Coordinates have been deposited in the Protein Data Bank with ID codes 1AS0, 1AS2, and 1AS3 for the GTPγS, GDP·P_i, and GDP complexes of $G^{42}VG_{i\alpha1}$.

RESULTS AND DISCUSSION

P-Loop Mutations in $G_{i\alpha1}$. Our initial interest was to understand the low k_{cat} for GTP hydrolysis by $G_{z\alpha}$ (0.02 min^{-1}) compared to those of many other G_α subunits (1−5 min^{-1}) (*21*, *31*, *32*). $G_{z\alpha}$ has a unique TSN sequence in the phosphate-binding loop (P-loop) rather than the consensus AGE sequence found in other G_α subunits, and this sequence was thus generated in $His_6G_{i\alpha1}$ (Figure 1A). Swapping the Ala^{41}, Gly^{42}, and Glu^{43} residues in $G_{i\alpha1}$ for the corresponding Thr, Ser, and Asn reduced the k_{cat} for GTP hydrolysis 17-fold. Examination of proteins with single mutations indicated that the change of $Gly^{42} \rightarrow$ Ser was responsible for the lower k_{cat} for GTP hydrolysis (Figure 1A).

$G^{42}VG_{i\alpha1}$ was next synthesized to investigate the effect of steric bulk versus a specific effect of the hydroxyl group in $G^{42}SG_{i\alpha1}$ (Figure 1B). The 30-fold reduction in k_{cat} observed (0.127 min^{-1}) is significant in two respects. First, it suggests that the comparatively low rate of GTP hydrolysis by $G_{z\alpha}$ may be due in part to the steric effects of Ser^{42}. More importantly, the $G^{42}VG_{i\alpha1}$ mutation mimics effects seen with $G^{12}V$ $p21^{ras}$. Structural studies of $G^{12}V$ $p21^{ras}$ have suggested that the Val^{12} side chain in the mutant protein pushes Gly^{60} and the catalytic Gln^{61} residues away from the γ-phosphate of GTP. However, it has been difficult to evaluate this hypothesis because the switch II region that contains Gln^{61} is poorly ordered in $p21^{ras}$. In contrast, the analogous Gln^{204} residue is situated in a well-ordered loop in the GTPγS·Mg^{2+} form of $G_{i\alpha1}$.

The GTPase activity of $G^{12}V$ $p21^{ras}$ cannot be stimulated by GAPs for this low-molecular-weight GTPase (*33*). We thus examined the interaction of the mutant $G_{i\alpha1}$ proteins with RGS4, a newly discovered GAP that stimulates the GTPase activity of all members of the $G_{i\alpha}$ subfamily of G_α

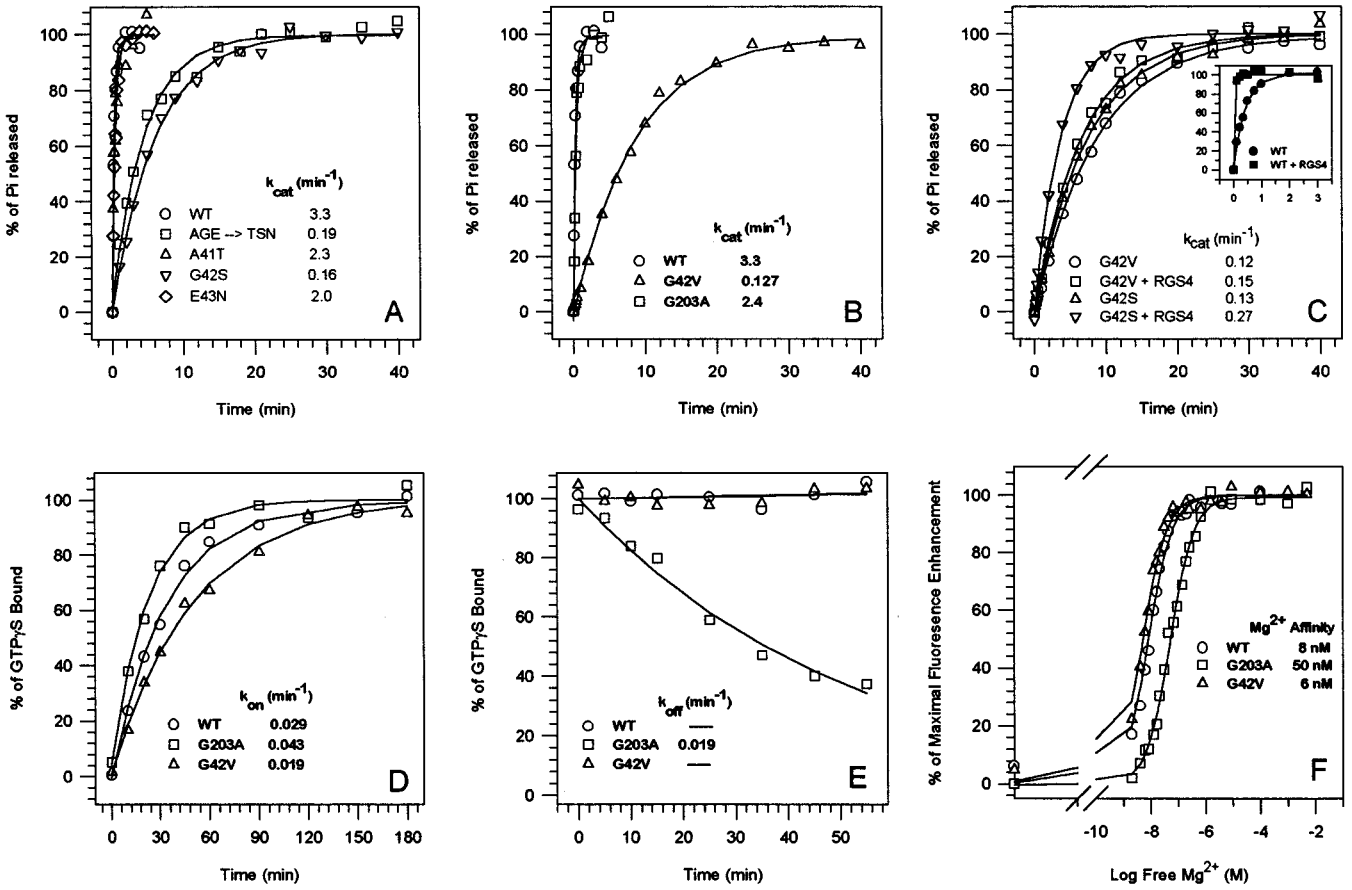

FIGURE 1: (A) Determination of k_{cat} for GTP hydrolysis by wild-type and mutant $G_{i\alpha1}$ proteins. Proteins were treated as described under Materials and Methods. P-loop mutants contained a hexahistidine sequence at their amino termini. Values are expressed as a percentage of the total $^{32}P_i$ generated during single turnover reactions for each protein. AGE → TSN corresponds to the triple mutant $A^{41}T$, $G^{42}S$, $E^{43}N$ in $G_{i\alpha1}$. (B) Determination of k_{cat} for GTP hydrolysis by $G^{42}V$ and $G^{203}A$ mutants of $G_{i\alpha1}$. Proteins were treated as described under Materials and Methods. Values are expressed as a percentage of the total $^{32}P_i$ generated during single turnover reactions for each protein. (C) Effect of RGS4 on the k_{cat} for GTP hydrolysis by $G^{42}V G_{i\alpha1}$ and $G^{42}S G_{i\alpha1}$. G_α proteins (100 nM) were mixed with RGS4 (400 nM) as described under Materials and Methods. Values are expressed as a percentage of the total $^{32}P_i$ generated during single turnover reactions for each protein. (D) [^{35}S]GTPγS binding kinetics. Proteins were treated as described under Materials and Methods. Values are expressed as a percentage of the maximal value of [^{35}S]GTPγS binding observed for each protein. (E) [^{35}S]GTPγS dissociation kinetics. Proteins were treated as described under Materials and Methods. Values are expressed as a percentage of the maximal value of [^{35}S]GTPγS binding observed for each protein. (F) Mg^{2+} binding affinities for $G_{i\alpha1}$(GTPγS) proteins. Proteins were treated as described under Materials and Methods. Values are expressed as a percentage of the maximum fluorescence enhancement observed for each protein.

subunits (*22*). The GTPase activity of $G^{42}V G_{i\alpha1}$ was not stimulated by RGS4 (Figure 1C). Interestingly, the GTPase activity of the less bulky $G^{42}S$ mutation was stimulated by RGS4, albeit modestly (2-fold at 400 nM RGS4). This parallels the observation that RGS4 can stimulate (by 6-fold) the GTPase activity of $G_{z\alpha}$ at comparable concentrations (*34*).

Biochemical Comparison of $G_{i\alpha1}$, $G^{42}V G_{i\alpha1}$, and $G^{203}A G_{i\alpha1}$. As mentioned, crystal structures of wild-type $G_{i\alpha1}$ in its GTPγS·Mg^{2+} (*14*) and GDP (*35*) forms have been described, as have the structures of $G^{203}A G_{i\alpha1}$ in the GDP·P_i and GDP forms (*17*). We have now crystallized $G^{42}V G_{i\alpha1}$ in all three states (GTPγS·Mg^{2+}, GDP·P_i, and GDP) and have compared the biochemical properties of the wild-type and mutant proteins in detail to facilitate analysis of their structures. The effects of these two mutations in $G_{s\alpha}$ are very similar (*36*); however, they differ importantly in the context of $G_{i\alpha1}$.

As demonstrated above (Figure 1B), $G^{42}V G_{i\alpha1}$ has a k_{cat} for GTP hydrolysis 30-fold lower than that of the wild-type protein, indicative of some structural perturbation of this protein's catalytic machinery. In contrast, $G^{203}A G_{i\alpha1}$ has a normal rate of GTP hydrolysis (2.4 min^{-1}) (Figure 1B).

G protein α subunits contain stoichiometric quantities of bound GDP. The rate of binding of GTP or GTPγS is limited by the rate of GDP dissociation. The similar [^{35}S]-GTPγS binding kinetics of wild-type and mutant proteins (Figure 1D) suggests that the mode of GDP binding for these proteins is essentially identical.

G_α subunits form a very high affinity complex with GTPγS·Mg^{2+}. Both $G_{i\alpha1}$ and $G^{42}V G_{i\alpha1}$ bind GTPγS quasi-irreversibly in the presence of the divalent cation (Figure 1E). By contrast, GTPγS dissociates from $G^{203}A G_{i\alpha1}$ with a rate of 0.019 min^{-1}. Binding of GTPγS·Mg^{2+} to $G^{203}A G_{i\alpha1}$ is thus somehow altered compared to the other two proteins. These observations are consistent with the fact that $G^{203}A G_{i\alpha1}$ and its homolog $G^{226}A G_{s\alpha}$ are unable to undergo the GTP-induced conformational change that causes dissociation of G_α from $G_{\beta\gamma}$ (*36*).

The steady-state rate for GTP hydrolysis at pH 8.0 (Hepes buffer) is essentially equal to the rate of GDP dissociation (as measured by the rate of GTPγS binding) (Table 4). Thus, the steady-state rate of catalysis by all three proteins is limited by product dissociation.

The fluorescence of tryptophan residues in $G_{i\alpha1}$ is enhanced by 30% upon exchange of GDP by GTPγS. The fluorescence of the resulting $G_{i\alpha1}$·GTPγS complex is further increased upon binding of Mg^{2+}. This effect was used to

Table 4: Steady-State GTPase Activity of Wild-Type and Mutant $G_{i\alpha1}$ Proteins

buffer	pmol of P_i/(pmol of protein·min)		
	wild-type	$G^{203}A$	$G^{42}V$
50 mM NaHEPES (pH 8.0)	0.027	0.045	0.017
50 mM NaH_2PO_4 (pH 8.0)	0.042	0.055	0.022
50 mM MES (pH 5.6)	0.072	0.104	0.035
50 mM NaH_2PO_4 (pH 5.6)	0.044	0.062	0.018

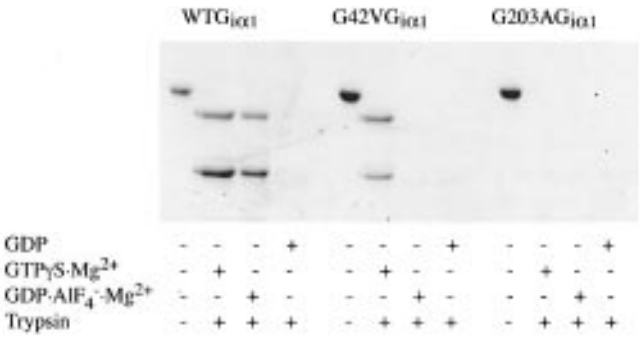

FIGURE 2: Trypsinization of wild-type and mutant $G_{i\alpha1}$ proteins. $G_{i\alpha1}$ proteins were incubated with either GDP, GTPγS + $MgSO_4$, or GDP + $MgSO_4$ + AlF_4^-, and with trypsin as indicated. Samples were resolved on a SDS−polyacrylamide gel and stained with Coomassie Blue as described under Materials and Methods.

monitor Mg^{2+} binding to the GTPγS forms of the proteins (Figure 1F). The apparent K_d for Mg^{2+} binding is the same for $G_{i\alpha1}$ (6 nM) and $G^{42}VG_{i\alpha1}$ (8 nM), whereas it is modestly diminished with $G^{203}AG_{i\alpha1}$ (50 nM). This is again consistent with the notion of an altered GTPγS·Mg^{2+} binding mode in $G^{203}AG_{i\alpha1}$.

Upon activation by GTPγS·Mg^{2+} or GDP·AlF_4^-·Mg^{2+}, $G_{i\alpha1}$ undergoes a conformational change that renders the protein resistant to proteolysis by trypsin. After rapid cleavage near the N-terminus, a 39-kDa species accumulates (*37*). By contrast, the inactive GDP-bound form of the protein is rapidly degraded. Both $G_{i\alpha1}$ and $G^{42}VG_{i\alpha1}$ are protected from tryptic digestion after incubation with GTPγS and Mg^{2+}, whereas $G^{203}AG_{i\alpha1}$ is not (Figure 2). This further corroborates the notion of a perturbed GTPγS·Mg^{2+} binding mode in $G^{203}AG_{i\alpha1}$. Interestingly, although $G^{42}VG_{i\alpha1}$ is protected against trypsin following activation by GTPγS·Mg^{2+}, it is not protected by AlF_4^-·Mg^{2+}. The $G_{i\alpha1}$·GDP·AlF_4^-·Mg^{2+} complex resembles the transition state for GTP hydrolysis (*14*). As might have been anticipated, this GTPase-deficient mutant appears to bind the transition state analog weakly.

Biochemical Characterization of the $G_{i\alpha1}$·GDP·P_i Complex. Both $G^{42}VG_{i\alpha1}$ and $G^{203}AG_{i\alpha1}$ have been crystallized in the GDP·P_i-bound state, while the wild-type protein has not (despite considerable effort). This raises questions about the stability of the GDP·P_i complex and the effect of the mutations on its lifetime and structure. Some have claimed that release of P_i from G_α proteins is slower than hydrolysis *per se* (*38*); others disagree (*39*).

We attempted to measure binding of $^{32}P_i$ to GDP·$G_{i\alpha1}$ (10 μM) by equilibrium dialysis at pH 8, 6, and 5.6 (to mimic crystallization conditions); binding was not detected. The K_d of P_i for GDP·$G_{i\alpha1}$ is thus significantly higher than 10 μM. The rate of steady-state hydrolysis of GTP by $G_{i\alpha1}$ and the two mutants studied here is limited by product (GDP) dissociation. Addition of phosphate at concentrations near

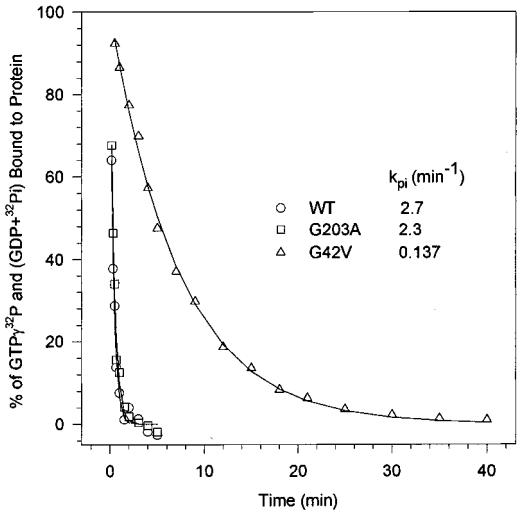

FIGURE 3: Determination of k_{pi} for GTP hydrolysis by $G^{42}VG_{i\alpha1}$ and $G^{203}AG_{i\alpha1}$. Proteins were treated as described under Materials and Methods. Values are expressed as a percentage of the maximal value of [γ-^{32}P]GTP binding observed for each protein.

or above its K_d for GDP·$G_{i\alpha1}$ should promote formation of GDP·P_i·$G_{i\alpha1}$ and reduce the steady-state rate of GTP hydrolysis. There was no inhibitory effect of 50 mM sodium phosphate at pH 8; very modest inhibition was observed at pH 5.6 (Table 4). It is thus unlikely that the K_d for P_i in the GDP·P_i·$G_{i\alpha1}$ complex is substantially less than 50 mM for either the wild-type or mutant proteins.

Values of k_{cat} for GTP hydrolysis reported above (Figure 1A,B) were determined by loading $G_{i\alpha1}$ proteins with [γ-^{32}P]-GTP and initiating hydrolysis by addition of Mg^{2+}. Reactions were quenched by addition of acidic charcoal to denature the protein and adsorb nucleotide. After removal of the charcoal, the amount of $^{32}P_i$ in the supernatant was quantified. The measurement thus includes both P_i released from the protein after hydrolysis and any P_i released from a GDP·P_i·$G_{i\alpha1}$ complex by denaturation. Hence, under these conditions, the k_{cat} rate constant measures the rate of γ-phosphate cleavage. As an alternative, single turnover GTPase reactions were quenched by dilution into cold buffer and rapid (<10 s) adsorption of protein to nitrocellulose membranes to quantify bound radioactive species, presumably both the GTP·$G_{i\alpha1}$ and the GDP·P_i·$G_{i\alpha1}$ species. The rate constant for the exponential decrease in the amount of radioactivity bound to the filter is defined as k_{pi} (Figure 3). Comparison of Figures 1B and 3 indicates that $k_{cat} = k_{pi}$ and thus, that release of P_i is fast relative to bond cleavage for both wild-type and mutant $G_{i\alpha1}$ proteins.

Overall Structure of $G^{42}VG_{i\alpha1}$. The fold of $G^{42}VG_{i\alpha1}$ is essentially identical to that of $G_{i\alpha1}$ (Figure 4A). The structure consists of two domains: a $p21^{ras}$-like guanine nucleotide-binding module, which spans residues 34−56 and residues 188−343, and an α-helical domain spanning residues 63−176. The switch regions are those segments that adopt different conformations in the active GTP and inactive GDP forms of $G_{i\alpha1}$. Switch I (residues 177−187) and switch II (residues 199−219) segments are involved in Mg^{2+} and γ-phosphate binding, respectively, as well as in catalysis. Both of these switch regions are present in most members of the $p21^{ras}$ superfamily. Switches III and IV are unique to G_α subunits. Switch III (residues 231−242) is a $\beta-\alpha$ turn that forms ionic contacts with switch II. Switch IV (residues

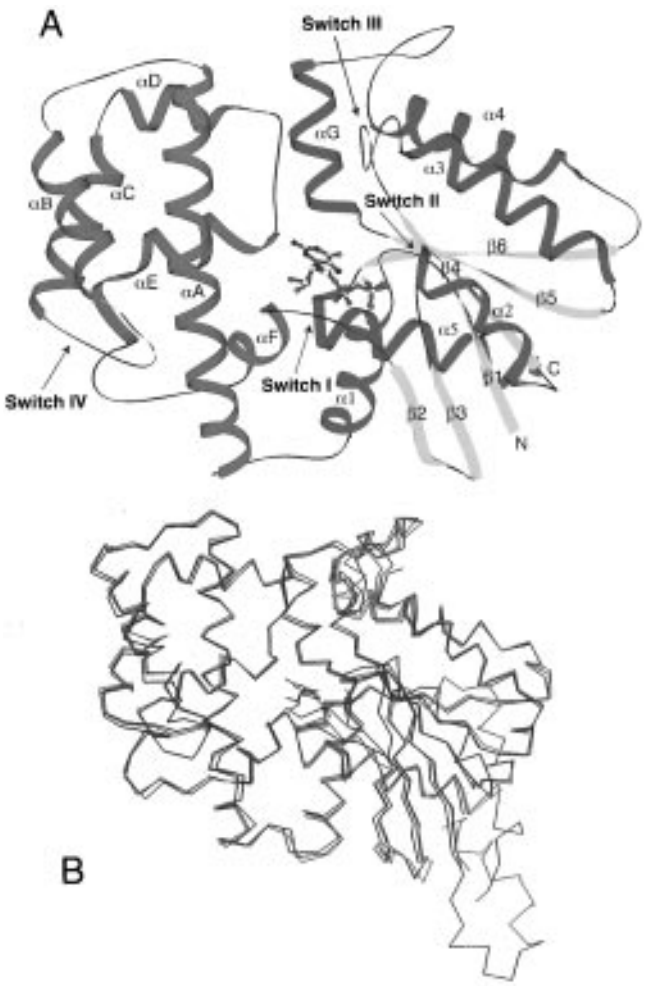

FIGURE 4: (A) Structure of $G_{i\alpha1}(GTP\gamma S{\cdot}Mg^{2+})$. The α-helical domain is colored red, and the ras-like domain is colored yellow (β-strands) and blue (α-helices). The $GTP\gamma S{\cdot}Mg^{2+}$ ligand is shown as a ball-and-stick model. N and C mark the positions of the first ordered residues at the amino (Val^{34}) and carboxyl (Leu^{343}) termini. The four switch regions are labeled. (B) Superposition of the Cα traces of $G^{42}VG_{i\alpha1}$ bound to $GTP\gamma S{\cdot}Mg^{2+}$ (blue), $GDP{\cdot}P_i$ (red), and GDP (green). The figure was generated using the program SETOR (43).

111−119) is a region that might be involved in oligomerization of $G_{i\alpha1}$(GDP) (*35*).

The structures of $G_{i\alpha1}$ and $G^{42}VG_{i\alpha1}$ in the $GTP\gamma S{\cdot}Mg^{2+}$ form are very similar; they can be superimposed with a rms (root mean square) deviation of 0.39 Å at Cα positions. Residues at the N-terminus (1−31) and C-terminus (345−354) are disordered in both structures. Similarly, the structures of $G^{42}VG_{i\alpha1}$ and $G^{203}AG_{i\alpha1}$ in the $GDP{\cdot}P_i$ form can be superimposed with a rms deviation of 0.23 Å at Cα positions. Like the structures of the $GTP\gamma S{\cdot}Mg^{2+}$ complex, residues at the N-terminus (1−31) and C-terminus (347−354) are also disordered in the $GDP{\cdot}P_i$ complex. Finally, the structures of $G_{i\alpha1}$ and $G^{42}VG_{i\alpha1}$ in the GDP form can be superimposed with a rms deviation of 0.24 Å at Cα positions. Unlike the $GTP\gamma S{\cdot}Mg^{2+}$ and $GDP{\cdot}P_i$ structures, however, the N-termini and C-termini form an ordered microdomain that is involved in quaternary interactions in crystals of $G_{i\alpha1}$(GDP).

Figure 4B depicts a superposition of the Cα traces of the $G^{42}VG_{i\alpha1}$ structures in the $GTP\gamma S{\cdot}Mg^{2+}$, $GDP{\cdot}P_i$, and GDP forms. The overall structures of these three complexes are similar. The rms deviation at Cα positions upon superposition of the $GTP\gamma S{\cdot}Mg^{2+}$ and $GDP{\cdot}P_i$ structures and upon superposition of the GDP and $GDP{\cdot}P_i$ structures are 1.70 and 0.58 Å, respectively. The intermediate $GDP{\cdot}P_i$ state more closely resembles the $GTP\gamma S{\cdot}Mg^{2+}$ structure in that both have disordered N- and C-termini as well as similar conformations of switch I. The conformation of switch II, however, is entirely different in the $GTP\gamma S{\cdot}Mg^{2+}$ and $GDP{\cdot}P_i$ structures, whereas it is disordered in the GDP structure. The switch III segment is poorly ordered in all three complexes. Interestingly, the switch IV region of the $GDP{\cdot}P_i$-bound protein, although not well ordered ($B/B_{av} = 1.8$),[2] more closely resembles that observed when GDP is bound, even though the $GDP{\cdot}P_i$-bound protein does not participate in homopolymeric interactions in the crystal lattice.

All of the contacts between the protein and the guanine nucleotide monophosphate moiety are similar in the three nucleotide-binding states of $G^{42}VG_{i\alpha1}$. In particular, noncovalent interactions of the α- and β-phosphates with residues 40−44 in the P-loop are conserved in the three structures and are identical to those seen in $G_{i\alpha1}$. However, during the course of hydrolysis, when the enzyme passes from the $GTP\gamma S{\cdot}Mg^{2+}$ to the $GDP{\cdot}P_i$ and eventually the GDP state, switch I and most notably switch II adopt different conformations to accommodate the bound ligands.

Structure of $G^{42}VG_{i\alpha1}(GTP\gamma S{\cdot}Mg^{2+})$. The active site of wild-type $G_{i\alpha1}(GTP\gamma S{\cdot}Mg^{2+})$ is shown in Figure 5A. A well-ordered water molecule is held in place by hydrogen bonds with the Thr^{181} main chain carbonyl and with the γ-phosphate oxygen. This water molecule is located 3.9 Å away from the γ-phosphorus and is positioned for in-line attack on the γ-phosphate. A Mg^{2+} cation with an octahedral coordination sphere is also present. The terminal oxygens of both the β- and γ-phosphates of GTPγS serve as ligands to this cation. Coordination of the γ-phosphate by Mg^{2+} should increase the electrophilicity of the GTP molecule for nucleophilic attack by the water. Furthermore, coordination of the β-phosphate should make the GDP molecule a better leaving group during γ-phosphate bond cleavage. Two additional ligands are the side chains of Thr^{181} and Ser^{47}. The remaining two axial coordination sites are occupied by water molecules. Also shown in Figure 5A is the switch II region, which spans a loop from Phe^{199} to Gly^{203} followed by an α-helical region from Gln^{204} to Cys^{214}. The single contact between the $GTP\gamma S{\cdot}Mg^{2+}$ ligand and switch II is the hydrogen bond between the Gly^{203} backbone nitrogen and the γ-phosphate oxygen. In addition, residues Glu^{236}, Asp^{237}, and Glu^{245} in switch III form ionic contacts with residues Arg^{205} and Arg^{208} in switch II. As demonstrated previously, Arg^{178} and Gln^{204} are critical participants in GTP hydrolysis but not GTP binding. These residues make no direct contacts with the GTPγS ligand or with other residues in the $G_{i\alpha1}$ protein. Nonetheless, they are positioned close to the β- and γ-phosphates. Slight movements of their side chains enable these residues to bind the transition state species and thereby catalyze GTP hydrolysis.

The structure of $G_{i\alpha1}$ with $GDP{\cdot}AlF_4^-{\cdot}Mg^{2+}$ as the bound ligand (Figure 6) closely approximates that of $G_{i\alpha1}(GTP\gamma S{\cdot}Mg^{2+})$ but with important differences. The γ-phosphate of

[2] B_{av} is the average B factor for all non-hydrogen atoms in the molecule. The B/B_{av} normalization facilitates comparison of thermal parameters of equivalent atoms in different crystal complexes.

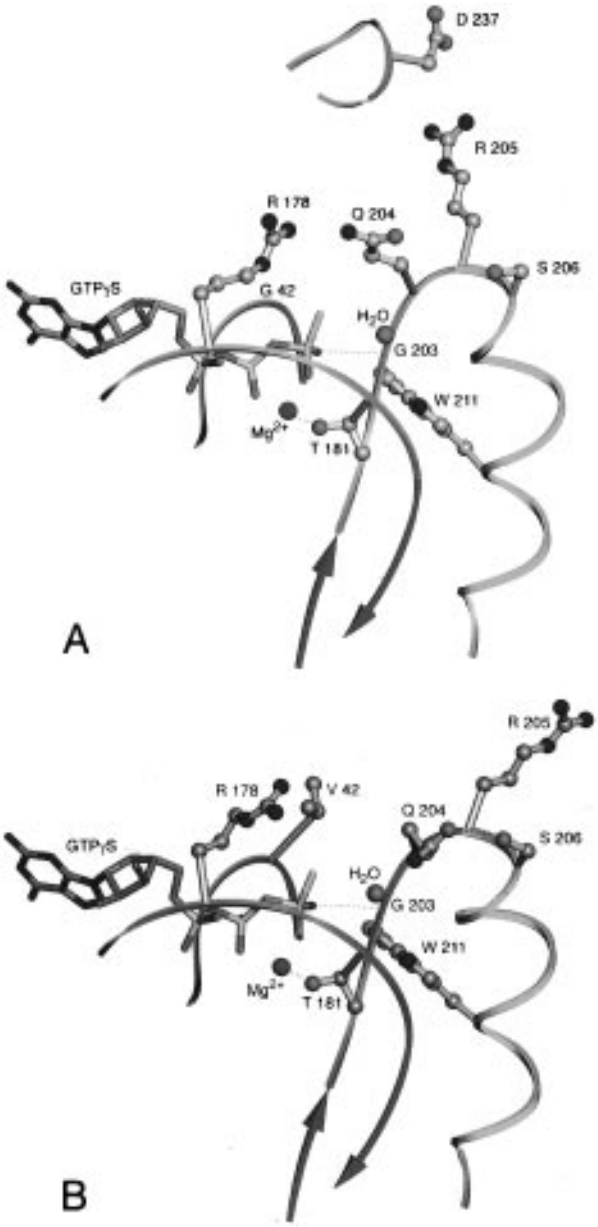

FIGURE 5: (A) Ribbon diagram of the $G_{i\alpha1}$(GTPγS·Mg^{2+}) active site. Helices are shown in yellow, β-strands are shown in light blue, and loops are shown in green. GTPγS·Mg^{2+} and relevant side chains are depicted as ball-and-stick models. Atoms are colored as follows: oxygen, red; nitrogen, blue; carbon, gray; magnesium, light blue; phosphorus, yellow; and sulfur, yellow. Selected hydrogen bonds are depicted as dashed lines. (B) Ribbon diagram of the $G^{42}VG_{i\alpha1}$(GTPγS·Mg^{2+}) active site. Note that the side chain of Arg^{205} is disordered and is modeled in an extended conformation.

GTPγS is replaced with an AlF_4^- moiety in which the octahedral coordination sphere of the Al^{3+} cation has four fluoride ligands in an equatorial plane. The remaining two axial coordination sites are occupied by a GDP β-phosphate oxygen and a water molecule. Furthermore, the Arg^{178} and Gln^{204} side chains have moved. The Arg^{178} side chain is within hydrogen-bonding distance of the fluoride ligands on Al^{3+}, and the Gln^{204} side chain is within hydrogen-bonding distance of both the nucleophilic water (or possibly hydroxide) (*40*) and a fluoride ligand on Al^{3+}. This species is reminiscent of the putative pentacoordinate trigonal bypyramidal transition state (or perhaps high energy intermediate) postulated to occur during γ-phosphate bond cleavage.

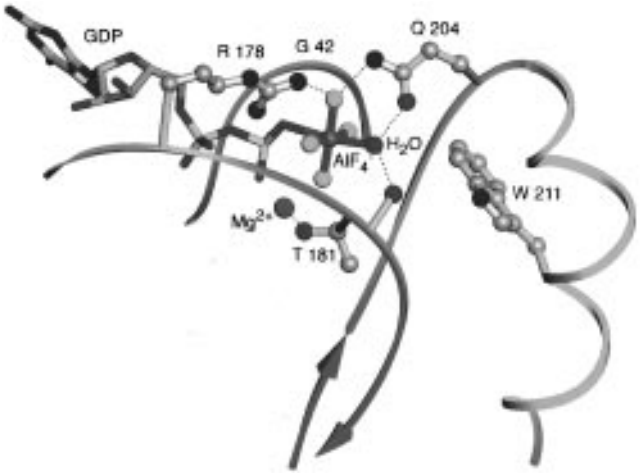

FIGURE 6: Ribbon diagram of the $G_{i\alpha1}$(GDP·AlF_4^-·Mg^{2+}) active site. Colors for ribbons and atoms are described in the legend of Figure 5. Aluminum and fluorine atoms are colored purple and yellow, respectively.

Hence, the complex is a transition state analog for GTP hydrolysis.

Model building using the active site of $G_{i\alpha1}$(GTPγS·Mg^{2+}) suggested that substitution of Gly^{42} in the P-loop with Val would result in significant steric interaction between the Val^{42} γ-methyl groups and the main and side chain atoms of Gln^{204} and this would force accommodation in the P-loop, switch II, or both. The structure of this mutant in the activated GTPγS·Mg^{2+} state is shown in Figure 5B. The conformation of the P-loop is unaltered. However, the steric bulk of the valine side chain has forced the peptide planes about residues 203−206 to rotate by as much as 30°. This, in turn, has pushed the Gln^{204} side chain out of the active site. Notably, the amide side chain of Gln^{204} is now well within hydrogen-bonding distance of Ser^{206} and is more ordered ($B/B_{av} = 1.4$ compared to 1.9 in the wild-type protein). On the other hand, the hydrogen bond between the Gly^{203} backbone nitrogen and the γ-phosphate oxygen is unaltered. These perturbations offer a clear rationale for the diminished GTPase activity of $G^{42}VG_{i\alpha1}$.

Interestingly, no electron density is visible for the side chain of Arg^{205} or for portions of switch III. Evidently, rotation of Arg^{205} has ruptured ionic contacts between its side chain and those of Asp^{237} and Glu^{245} in switch III as well as the hydrogen bond between the Arg^{205} backbone nitrogen and the Glu^{239} side chain carboxylate. Rotation about the Arg^{205} main chain has thus severed important contacts between switch II and switch III. This, in turn, has resulted in a highly mobile switch III region in the structure of the activated mutant protein.

The P-loop region forms hydrogen bonds with the α- and β-phosphates of the guanine nucleotide, whereas the Gly^{203} backbone amide is hydrogen bonded to the γ-phosphate. Since these contacts are all unaltered in $G^{42}VG_{i\alpha1}$-(GTPγS·Mg^{2+}), it is not surprising that both wild-type and $G^{42}VG_{i\alpha1}$ bind GTPγS·Mg^{2+} irreversibly (Figure 1E) and are protected from tryptic proteolysis when so activated (Figure 2). Furthermore, the conformation of the Ser^{47} and Thr^{181} ligands in the Mg^{2+} coordination sphere are unaltered by the $G^{42}V$ mutation, consistent with the strong affinity of both the wild-type and mutant proteins for Mg^{2+} (Figure 1F).

Although the structure of $G^{203}AG_{i\alpha1}$(GTPγS·Mg^{2+}) has not been elucidated, replacement of a hydrogen atom by a methyl

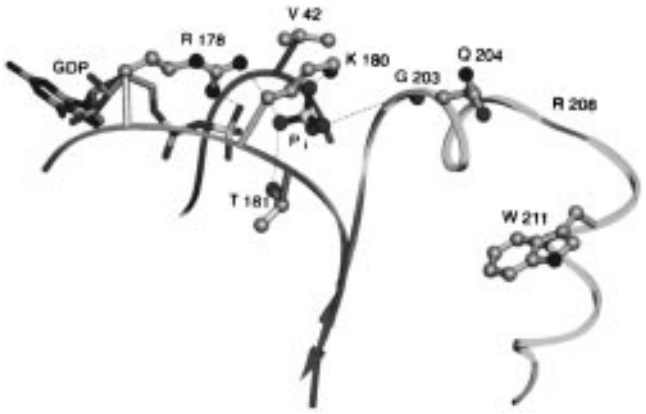

FIGURE 7: Ribbon diagram of the $G^{42}VG_{i\alpha1}(GDP{\cdot}P_i)$ active site. Colors for ribbons and atoms are described in the legend of Figure 5.

group on Gly^{203} in the native structure would cause a steric clash between the Ala^{203} side chain and the Gly^{42} main chain (the glycine ϕ and ψ angles fall within allowed regions for non-glycine side chains). This should result in a conformational change in the P-loop or, more likely, in the contact between Ala^{203} and the γ-phosphate. This may account for the diminished affinity of $G^{203}AG_{i\alpha1}$ for $GTP\gamma S{\cdot}Mg^{2+}$ (Figure 1E), as well as its susceptibility toward trypsinolysis even when $GTP\gamma S{\cdot}Mg^{2+}$ is bound (Figure 2). Furthermore, the altered nucleotide binding mode of $G^{203}AG_{i\alpha1}$ might also account for the modestly diminished affinity of the protein for Mg^{2+} (Figure 1F).

Structure of $G^{42}VG_{i\alpha1}(GDP{\cdot}P_i)$. Hydrolysis of GTP by $G_{i\alpha1}$ results in formation of a transient, $GDP{\cdot}P_i$-bound intermediate. The structure of a complex between $G^{42}VG_{i\alpha1}$ and $GDP{\cdot}P_i$ is shown in Figure 7. The once terminal γ-phosphorus atom has moved 2.2 Å away from the GDP β-phosphorus. The structure of $G^{42}VG_{i\alpha1}(GTP\gamma S{\cdot}Mg^{2+})$ indicates that translation of the γ-phosphate by this distance would cause steric clashes with main chain atoms of switch I (Thr^{181}) and switch II (Gly^{202} and Gly^{203}). In fact, the protein has undergone substantial conformational changes in these regions to accommodate the bound phosphate ion in the $GDP{\cdot}P_i$ complex.

Although the conformation of the switch I main chain is similar to that in the $GTP\gamma S{\cdot}Mg^{2+}$ complex, residues 178−183 have moved approximately 1.0 Å away from the active site to alleviate the steric contact with the phosphate ion. Furthermore, the Thr^{181} side chain has rotated 90° to form a hydrogen bond with an oxygen of P_i. The side chain of Lys^{180} is reoriented from a solvent-exposed position in the $GTP\gamma S{\cdot}Mg^{2+}$ complex to one in which the amine moiety forms a hydrogen bond with a P_i oxygen atom. Arg^{178} also moves from a poorly ordered, solvent-exposed position ($B/B_{av} = 1.3$) to one in which it forms strong ionic contacts ($B/B_{av} = 0.70$) with both the GDP β-phosphate and the P_i oxygen atoms.

The Mg^{2+} binding site also appears to be dismantled in the $GDP{\cdot}P_i$ complex. In part, this results from the reorientation of the Thr^{181} side chain, a ligand for the Mg^{2+} cation. In addition, under the conditions of crystallization (pH 5.5−5.8), the GDP β-phosphate and the free phosphate ions are each expected to carry a single negative charge. This would reduce electrostatic repulsion between the GDP and P_i anions, with consequent stabilization of the $GDP{\cdot}P_i$ complex; this intermediate might be considerably less stable at neutral pH. Protonation of these ligands would also reduce their ability to coordinate Mg^{2+}, and this may account for the absence of a Mg^{2+} cation in the active site.

The most significant conformational changes are observed in the switch II α-helix. In both wild-type and $G^{42}VG_{i\alpha1}$-$(GTP\gamma S{\cdot}Mg^{2+})$, the switch II region spans a loop from Phe^{199} to Gly^{203}, followed by an α-helical segment from Gln^{204} to Cys^{214}. In the $GDP{\cdot}P_i$ intermediate, two helical segments are evident. One α-helix spans residues Gly^{203} to Lys^{207} and the other spans residues Lys^{209} to Phe^{215}. Arg^{208} forms a kink between these two α-helices. The formation of these two helices has several important consequences. First, this conformational change has, in effect, pulled the switch II region away from the active site, creating a binding site for P_i. The hydrogen bond between the Gly^{203} main chain nitrogen and the free P_i oxygen atom is maintained by the altered conformation of switch II. Furthermore, the dipole of the first helical segment is directed toward the phosphate ion. The second helical segment has also rotated by 180° such that Trp^{211} (responsible for $GTP\gamma S{\cdot}Mg^{2+}$-induced fluorescence) moves from a hydrophobic interface with the α3 helix in the $GTP\gamma S{\cdot}Mg^{2+}$ structure to a more solvent-exposed site in the $GDP{\cdot}P_i$ complex. Furthermore, this α-helix was buried against the α3 helix and sitting between the β1 and β3 strands in the $GTP\gamma S{\cdot}Mg^{2+}$ structure; in the $GDP{\cdot}P_i$ complex it has moved toward the α3 helix, placing it just above the β1 strand (not shown). Finally, these rearrangements have pushed the catalytic Gln^{204} residue out of the active site into a highly mobile, solvent-exposed position.

The conformational changes in switch II move the Arg^{205} and Arg^{208} side chains into more solvent-exposed regions, away from any possible contacts with switch III. Since these contacts may account for the rigidity of switch III in the $G_{i\alpha1}(GTP\gamma S{\cdot}Mg^{2+})$ structure, their loss in the $G^{42}VG_{i\alpha1}$-$(GDP{\cdot}P_i)$ complex results in a switch III region that is partially disordered and pushed away from the active site.

The structures of $G^{203}AG_{i\alpha1}(GDP{\cdot}P_i)$ and $G^{42}VG_{i\alpha1}$-$(GDP{\cdot}P_i)$ are essentially the same, despite their disparate biochemical properties. Although both mutations perturb the active site, the observation of identical $GDP{\cdot}P_i$-bound species suggests that the structures represent a conformation that occurs only transiently in the wild-type protein but is somehow stabilized by each of the two mutations.

The active sites of the $G^{203}A$ and $G^{42}V$ mutants are shown in greater detail in Figure 8 to suggest a common mechanism for stabilization of the $GDP{\cdot}P_i$ intermediate. For $G^{203}AG_{i\alpha1}$-$(GDP{\cdot}P_i)$, a van der Waals contact between the methyl group of Ala^{203} and the main chain nitrogen of Gly^{42} may be sufficient to push the amino terminus of switch II out of the P_i binding pocket. Analogously, the $G^{42}VG_{i\alpha1}(GDP{\cdot}P_i)$ structure reveals a potential contact between the Val^{42} side chain and the Gly^{203} main chain. Although the distance is large for a van der Waals interaction, one must consider that the amino terminus of switch II is conformationally constrained. Hence, both the $G^{42}V$ and $G^{203}A$ mutations may force the switch II peptide segment into one of a limited number of possible conformations that permits creation of a phosphate-binding pocket. In the wild-type structure, there are no potential van der Waals contacts between the P-loop and the N-terminus of switch II; the switch II peptide segment is free to adopt conformations that would exclude

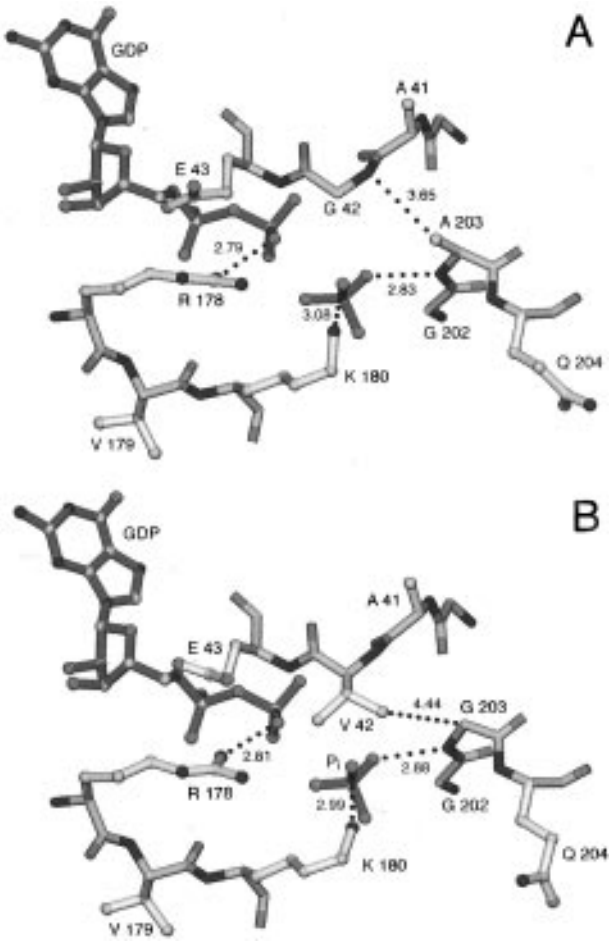

FIGURE 8: (A) Ball-and-stick model of the $G^{203}AG_{i\alpha1}$(GDP·P_i) active site. Colors for atoms are described in the legend of Figure 5. The GDP and P_i ligands are highlighted in green. Hydrogen bonds and potential van der Waals contacts are depicted by dotted lines. (B) Ball-and-stick model of the $G^{42}VG_{i\alpha1}$(GDP·P_i) active site.

P_i from the active site, thereby limiting the stability of the $G_{i\alpha1}$(GDP·P_i) complex.

An alternative explanation for the stability of the GDP·P_i intermediate in these mutants rests on the observation that the $G^{12}V$ and $G^{60}A$ mutations in $p21^{ras}$ (G^{60} is analogous to G^{203} in $G_{i\alpha1}$) alter the pK_a of the GTP γ-phosphate (*41*). Conceivably, the Ala^{203} or Val^{42} side chains in the $G_{i\alpha1}$ mutants may alter the pK_a's of the GDP β-phosphate and the free P_i such that their resultant protonation states increase the stability of the GDP·P_i entity. Nevertheless, it must be stressed that the GDP·P_i intermediate is not stable in either the wild-type or the mutant proteins (Table 4) nor is release of P_i rate limiting (Figure 3). Additional factors that may facilitate the crystallization of this species are the high phosphate concentrations utilized (~2 M), driving the equilibrium toward the GDP·P_i species, and the acidic pH (5.5−5.8), which reduces the electrostatic repulsion between the GDP β-phosphate and P_i.

Structure of $G^{42}VG_{i\alpha1}$(GDP). Upon release of phosphate from the $G^{42}VG_{i\alpha1}$(GDP·P_i) intermediate, the protein assumes its inactive GDP-bound state (Figure 9). As a result of the loss of contacts with P_i, switch I moves away from the active site by 2.0 Å and the side chains of Lys^{180} and Thr^{181} become disordered. Only the Arg^{178} side chain of switch I forms a contact with the α- and β-phosphates of GDP. These conformational changes also dismantle the Mg^{2+}-binding site.

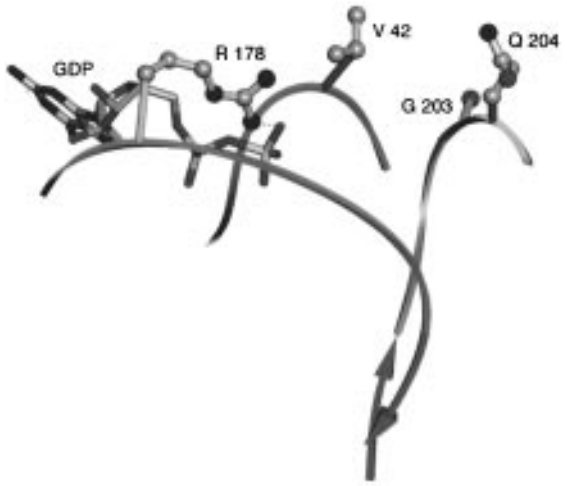

FIGURE 9: Ribbon diagram of the $G^{42}VG_{i\alpha1}$(GDP) active site. Colors of ribbons and atoms are described in the legend of Figure 5.

In contrast to $p21^{ras}$, GDP·$G_{i\alpha}$ proteins have low affinity for Mg^{2+}.

Dissociation of P_i ruptures the hydrogen bond between the main chain nitrogen of Gly^{203} and the free phosphate ion oxygen, thereby removing the only contact between switch II and the nucleotide. Switch II thus assumes a highly mobile conformation with no discernible electron density for residues 205−215. This collapse of switch II upon inactivation is characteristic of several other GTPases, including $p21^{ras}$. Finally, switch III also becomes disordered as a result of the loss of stabilizing contacts with switch II.

No electron density is visible for residues 202−217 in the switch II region of $G_{i\alpha1}$(GDP). However, electron density is clearly visible for the main chain atoms of residues 202−204 in $G^{42}VG_{i\alpha1}$(GDP). The conformation adopted by these three residues closely resembles that of the amino terminus of the first helical segment of the GDP·P_i complex. This is consistent with the proposed mechanism by which the $G^{203}A$ and $G^{42}V$ mutations stabilize the GDP·P_i intermediate, since this model also predicts that the Val^{42} or Ala^{203} side chains of these mutants may also limit the conformational flexibility of switch II in the inactive GDP-bound protein. This also suggests that the switch II conformation seen in the GDP·P_i complex is not solely the result of low pH, since crystals of $G^{42}VG_{i\alpha1}$(GDP) were obtained at neutral pH. Apart from this small difference, the inactive GDP complex is identical in wild-type and mutant proteins. These similarities account for their similar rates of GDP dissociation (Figure 1D).

Conclusions. Both $G^{42}VG_{i\alpha1}$ and $G^{12}V$ $p21^{ras}$ have diminished rates of GTP hydrolysis, and neither rate can be increased by appropriate GAPs. Unlike $p21^{ras}$, the structure of the well-ordered switch II region of $G^{42}VG_{i\alpha1}$(GTPγS·Mg^{2+}) provides a clear rationale for the diminished k_{cat} for GTP hydrolysis. The bulk of the Val^{42} side chain forces the side chain of Gln^{204} into a catalytically incompetent conformation. These findings substantiate the original models for $p21^{ras}$ proposed by Wittinghofer (*12*) and Privé (*11*). Similarly, the bulk of the unique Ser^{42} residue in $G_{z\alpha}$ may also account for the comparatively slow rate of GTP hydrolysis that characterizes this G_α subunit. Interestingly, RGS4 can stimulate the GTPase activity of $G^{42}SG_{i\alpha1}$, albeit to a modest level, perhaps because of the smaller bulk of the Ser residue. This parallels the observation that RGS4 can stimulate the GTPase activity of $G_{z\alpha}$.

Crystallographic studies with $G^{42}VG_{i\alpha1}$ demonstrate that the switch I and the switch II regions of the protein undergo significant conformational changes upon hydrolysis of GTP to a transient GDP·P_i intermediate. It must be emphasized that most of these changes center around the switch II region. Eventual release of P_i from $G^{42}VG_{i\alpha1}$(GDP·P_i) generates $G^{42}VG_{i\alpha1}$(GDP). During this second transition along the reaction coordinate, the switch I segment moves further from the active site and switch II adopts a highly mobile conformation.

Although these studies were performed with a mutant $G^{42}VG_{i\alpha1}$ subunit with an altered GTPγS·Mg^{2+} binding site, we believe that the results are not artifacts of the mutation for the following reasons: (1) The $G^{42}V$ mutation in $G_{i\alpha1}$ impairs catalytic activity but does not affect affinity for nucleotide. The reverse is true of the $G^{203}AG_{i\alpha1}$ mutant. Thus, even though $G^{42}VG_{i\alpha1}$ and $G^{203}AG_{i\alpha1}$ have very different biochemical properties, they possess essentially identical structures when bound to GDP·P_i and GDP. (2) The affinity of both wild-type and mutant proteins for P_i in the GDP·P_i complex is low, and release of P_i is significantly faster than cleavage of the γ-phosphate. Thus, we believe that the structure of the GDP·P_i-bound intermediate in $G^{42}VG_{i\alpha1}$ and $G^{203}AG_{i\alpha1}$ represents a conformation that occurs transiently in the wild-type protein; it is somehow stabilized by these mutations, perhaps by limiting the conformational flexibility of switch II.

The only other study that closely resembles our own is the structural characterization of the ATPase fragment of the bovine 70-kDa heat shock protein in its ATP- and ADP·P_i-bound forms. Here, McKay and co-workers (*42*) have seen active site rearrangements that resemble those described above. Like $G_{i\alpha1}$, this enzyme also catalyzes slow γ-phosphate cleavage (<1 min^{-1}). It is quite possible that in both the ATPase fragment and the $G_{i\alpha1}$ subunit, extensive reorganization of the active site contributes to the energy barrier during γ-phosphate cleavage and thereby accounts, in part, for the poor catalytic efficiency of these enzymes.

ACKNOWLEDGMENT

We thank Mark Mixon, John Tesmer, Bryan Sutton, and the staff at the Cornell High Energy Synchrotron Source (CHESS) for assistence with data collection and Linda Hannigan and Marian Stanzel for excellent technical assistance.

REFERENCES

1. Gilman, A. G. (1987) *Annu. Rev. Biochem. 56*, 615−649.
2. Simon, M. I., Strathmann, M. P., & Gautam, N. (1991) *Science 252*, 802−808.
3. Hepler, J. R., & Gilman, A. G. (1992) *Trends Biochem. Sci. 17*, 383−387.
4. Bourne, H. R., Sanders, D. A., & McCormick, F. (1991) *Nature 349*, 117−127.
5. Sprang, S. R. (1997) *Annu. Rev. Biochem. 66*, 639−678.
6. Wall, M. A., Coleman, D. E., Lee, E., Iniguez-Lluhi, J. A., Posner, B. A., Gilman, A. G., & Sprang, S. R. (1995) *Cell 83*, 1047−1058.
7. Cassel, D., & Selinger, Z. (1977) *Proc. Natl. Acad. Sci. U.S.A. 74*, 3307−3311.
8. Barbacid, M. (1987) *Annu. Rev. Biochem. 56*, 779−828.
9. Seeburg, P. H., Colby, W. W., Capon, D. J., Goeddel, D. V., & Levinson, A. D. (1984) *Nature 312*, 71−75.
10. Pai, E. F., Kabsch, W., Krengel, U., Holmes, K. C., John, J., & Wittinghofer, A. (1989) *Nature 341*, 209−214.
11. Prive, G. G., Milburn, M. V., Tong, L., deVos, A. M., Yamaizumi, Z., Nishimura, S., & Kim, S.-H. (1992) *Proc. Natl. Acad. Sci. U.S.A. 89*, 3649−3653.
12. Krengel, U., Schlichting, I., Scherer, A., Schumann, R., Frech, M., John, J., Kabsch, W., Pai, E. F., & Wittinghofer, A. (1990) *Cell 62*, 539−548.
13. Graziano, M. P., & Gilman, A. G. (1989) *J. Biol. Chem. 264*, 15475−15482.
14. Coleman, D. E., Berghuis, A. M., Lee, E., Linder, M. E., Gilman, A. G., & Sprang, S. R. (1994) *Science 265*, 1405−1412.
15. Noel, J. P., Hamm, H. E., & Sigler, P. B. (1993) *Nature 366*, 654−663.
16. Casey, P. J., Fong, H. K. W., Simon, M. I., & Gilman, A. G. (1990) *J. Biol. Chem. 265*, 2383−2390.
17. Berghuis, A. M., Lee, E., Raw, A. S., Gilman, A. G., & Sprang, S. R. (1996) *Structure 4*, 1277−1290.
18. Kunkel, T. A., Roberts, J. D., & Zabour, R. A. (1987) *Methods Enzymol. 154*, 367−382.
19. Lee, E., Linder, M. E., & Gilman, A. G. (1994) *Methods Enzymol. 237*, 146−164.
20. Northup, J. K., Smigel, M. D., & Gilman, A. G. (1982) *J. Biol. Chem. 257*, 11416−11423.
21. Higashijima, T., Ferguson, K. M., Smigel, M. D., & Gilman, A. G. (1987) *J. Biol. Chem. 262*, 757−761.
22. Berman, D. M., Wilkie, T. M., & Gilman, A. G. (1996) *Cell 86*, 445−452.
23. Higashijima, T., Ferguson, K. M., Sternweis, P. C., Ross, E. M., Smigel, M. D., & Gilman, A. G. (1987) *J. Biol. Chem. 262*, 752−756.
24. Sternweis, P. C., & Robishaw, J. D. (1984) *J. Biol. Chem. 259*, 13806−13813.
25. Coleman, D. E., Lee, E., Mixon, M. B., Linder, M. E., Berghuis, A. M., Gilman, A. G., & Sprang, S. R. (1994) *J. Mol. Biol. 238*, 630−634.
26. Otwinowski, Z. (1993) in *Data Collection and Processing* (Sawyer, L., Isaacs, N., & Bailey, S., Eds.) pp 56−62, Science and Engineering Research Council, Warrington, U.K.
27. Brunger, A. T. (1992) in *X-PLOR Version 3.1. A System for X-ray Crystallography and NMR*, Yale University Press, New Haven, CT.
28. Read, R. J. (1986) *Acta Crystallogr. A42*, 140−149.
29. Jones, T. A., Bergdoll, M., & Kjeldgaard, M. (1990) in *Crystallographic and Modeling Methods in Molecular Design* (Bugg, C. E., & Ealick, S. E., Eds.) pp 189−199, Springer Verlag, New York.
30. Laskowski, R. A., MacArthur, M. W., Moss, D. S., & Thornton, J. M. (1993) *J. Appl. Crystallogr. 26*, 283−291.
31. Graziano, M. P., Freissmuth, M., & Gilman, A. G. (1989) *J. Biol. Chem. 264*, 409−418.
32. Linder, M. E., Ewald, D. A., Miller, R. J., & Gilman, A. G. (1990) *J. Biol. Chem. 265*, 8243−8251.
33. Trahey, M., & McCormick, F. (1987) *Science 238*, 542−545.
34. Berman, D. M., Kozasa, T., & Gilman, A. G. (1996) *J. Biol. Chem. 271*, 27209−27212.
35. Mixon, M. B., Lee, E., Coleman, D. E., Berghuis, A. M., Gilman, A. G., & Sprang, S. R. (1995) *Science 270*, 954−960.
36. Lee, E., Taussig, R., & Gilman, A. G. (1992) *J. Biol. Chem. 267*, 1212−1218.
37. Fung, B. K.-K., & Nash, C. R. (1983) *J. Biol. Chem. 258*, 10503−10510.
38. Ting, T. D., & Ho, Y.-K. (1991) *Biochemistry 30*, 8996−9007.
39. Guy, P. M., Koland, J. G., & Cerione, R. A. (1990) *Biochemistry 29*, 6954−6964.
40. Schweins, T., & Warshel, A. (1996) *Biochemistry 35*, 14232−14243.
41. Schweins, T., Geyer, M., Kalbitzer, H. R., Wittinghofer, A., & Warshel, A. (1996) *Biochemistry 35*, 14225−14231.
42. Flaherty, K. M., Wilbanks, S. M., DeLuca-Flaherty, C., & McKay, D. B. (1994) *J. Biol. Chem. 269*, 12899−12907.
43. Evans, S. V. (1993) *J. Mol. Graphics 11*, 134−138.

BI971912P